Surpassing the Nyquist Sampling Limit via Postmodulation

Qi Song ,[‡] Binke Xia ,[‡] Jingzheng Huang,[*] Tailong Xiao , Hongjing Li, and Guihua Zeng[†]

State Key Laboratory of Advanced Optical Communication Systems and Networks, School of Electronic Information and Electrical Engineering, Institute of Quantum Sensing and Information Processing, Shanghai Jiao Tong University, Shanghai 200240, People's Republic of China

Surpassing the Nyquist sampling limit to avoid aliasing distortion is an important issue for the task of time-varying parameter estimation. To achieve this goal, we propose a high-precision time-varying parameter estimation scheme based on split detection and postmodulation of light instead of postprocessing of data. Theoretical analysis demonstrates its advantage of surpassing the Nyquist sampling limit and the avoidance of anti-aliasing distortion. In order to illustrate the feasibility, a numerical simulation based on the acceptance rejection sampling method is performed showing the noise robustness of the scheme in terms of correlation coefficient, root-mean-square error, and mean absolute error. Our scheme provides a method for function estimation.

I. INTRODUCTION

In order to measure a time-varying parameter, one applies a physical process to convert the parameter to a signal for detection. To avoid aliasing distortion, the responses of detection devices are required to be fast enough compared with the signal frequencies. According to the Nyquist sampling theorem, the sampling frequency of a detector should be at least twice the maximum signal frequency component, otherwise the signal quality will be damaged by aliasing distortions [1–3]. For example, immersive sound quality will be destroyed by frequency aliasing distortion in an audio object [4,5], and image information distortion will appear in photoelectric imaging [6].

Many efforts have been made to suppress the problem of aliasing distortion caused by insufficient detection bandwidth. One solution uses the prior information of the signal to be measured. For example, an anti-aliasing filter filters out the high-frequency components higher than half of the sampling frequency [7,8] and compressed sensing can sample the signal at sub-Nyquist rate based on the sparsity and incoherence of the signal [9–14]. However, these methods can only overcome the limitation on sampling frequency to a certain extent. Other solutions can surpass the Nyquist sampling limit in time-domain sampling with limitation. For example, the time-shifted multicoset sampling strategy [15–17] is limited by the width of practical analog-to-digital conversion and the bandwidth of signal subbands

is limited by the width of modulated signals and filters in the modulated wideband converter method [17].

In this work, a high-precision time-varying parameter estimation scheme based on weak measurement is proposed to surpass the Nyquist sampling limit without suffering aliasing distortions. Different from previous proposals, in this scheme the signal sampling is performed in the frequency domain instead of the time domain, and realized by postmodulation of light instead of postprocessing of data. Moreover, it is numerically demonstrated that this scheme is robust to white noise.

This paper is organized as follows. In Sec. II, the theoretical model of our scheme is built up and analyzed, where theoretical analysis highlights why and how it can surpass the Nyquist sampling limit. In order to illustrate the feasibility of our scheme, a further theoretical analysis is performed and a numerical simulation based on the acceptance rejection sampling method is described in Sec. III A. In Sec. III B, the influence of white noise on our scheme is analyzed. Finally, discussions and conclusions are presented in Sec. IV.

II. PRINCIPLE

First of all, we focus on signal sampling and the Nyquist sampling limit. For any detector that measures a signal in the time domain, there exists a minimum temporal duration $T_{d(\min)}$ for completing a single-shot detection. In consequence, the maximum frequency of signal sampling is $f_{d(\max)} = 1/T_{d(\min)}$ by this detector. In order to avoid any aliasing distortion, the maximum frequency component of the signal, which is denoted by $f_{s(\max)}$, should be

---

[*]jzhuang1983@sjtu.edu.cn

[†]ghzeng@sjtu.edu.cn

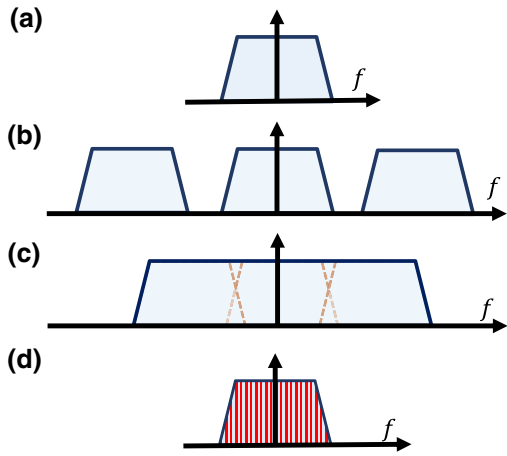[‡]These authors contributed equally to this work.

FIG. 1. Schematic diagram of frequency spectrum in different sampling frequency or sampling domain. (a) The original spectrum of the time-varying signal. (b) The frequency spectrum obtained by sampling the signal in the time domain when the detection frequency satisfies the Nyquist sampling theorem. (c) The overlapped frequency spectrum that is obtained by sampling the signal in the time domain with the frequency lower than twice the maximum frequency of the signal. The trapezoid surrounded by solid blue lines indicates the aliased signal spectrum, which is formed by trapezoids surrounded by orange dotted lines. (d) The signal spectrum sampled in the frequency domain, where the red lines represent the frequency sampling points.

limited by [1–3]

$$f_{s(max)} \leq \frac{1}{2} f_{d(max)}. \qquad (1)$$

For example, consider a time-varying signal with frequency spectrum depicted in Fig. 1(a). If this signal is sampled by a high enough frequency, its frequency spectrum can be perfectly estimated from the detection results, as is shown in Fig. 1(b). On the other hand, if the sampling frequency is lower than $2f_{s(max)}$, the frequency components will be overlapped, as shown in Fig. 1(c).

Alternatively, the signal can be revealed from its frequency spectrum $G(f)$. In this case, the signal sampling is performed in the frequency domain, as shown in Fig. 1(d). To perfectly reconstruct $g(t)$, two conditions should be satisfied. The first condition requires the sampling interval Δf to be small enough, which can be easily fulfilled. Note that $\Delta f \leq 1/T_{d(min)}$ [2], so that Δf can be set arbitrarily small. The second condition requires the sampling range to exceed the full frequency spectrum, which is also true because we can always find an integer k to make $k\Delta f > f_{s(max)}$. In consequence, if one tries to reveal the signal by performing sampling in the frequency domain, the maximum frequency component of the signal is in principle not limited:

$$f_{s(max)} \to \infty, \qquad (2)$$

which surpasses the Nyquist sampling limit given by Eq. (1).

However, sampling a signal in the frequency domain is very difficult to realize by direct data processing [2,3,18], as is shown in Fig. 2(a). To solve this problem, we propose a scheme involving performing postmodulations of the predetected signal rather than postprocessing of the detected data. Our scheme begins with encoding the time-varying signal to a physical parameter via a weak interaction between a two-level ancillary system and a continuous variable pointer [19,20] [see Fig. 2(b)]:

$$\hat{U} = e^{-ig(t)\hat{A}\otimes\hat{p}}, \qquad (3)$$

where $\hat{A}$ and $\hat{p}$ are two observables of the system and pointer, respectively, and the coupling strength $g(t)$ is proportional to the value of the signal. Moreover, the initial states of the system and pointer are denoted as $|i\rangle = (1/\sqrt{2})(|0\rangle + |1\rangle)$ and $|\phi_i\rangle$, respectively, and $g(t)$ satisfies $|g(t)| \langle\phi_i|\hat{p}|\phi_i\rangle \ll 1$. The weak interaction process can approximate to first order:

$$\hat{U} \approx \hat{I} - ig(t)\hat{A} \otimes \hat{p}. \qquad (4)$$

And then the system is projected to a postselected state of $|f\rangle = (1/\sqrt{2})\left(e^{i\varepsilon}|0\rangle + e^{-i\varepsilon}|1\rangle\right)$ with ε being a phase factor. The final pointer state becomes

$$|\phi_f(t)\rangle = [\langle f|i\rangle - ig(t)\langle f|\hat{A}|i\rangle\hat{p}]|\phi_i\rangle. \qquad (5)$$

In consequence, the value of observable $\hat{p}$ is given by $p_f(t) = \langle\phi_f(t)|\hat{p}|\phi_f(t)\rangle/\langle\phi_f(t)|\phi_f(t)\rangle$.

Directly estimating the parameter of interest requires a detection speed faster than twice the varying speed of $g(t)$, which suffers from the Nyquist sampling limit problem. To avoid this problem, a split postmodulation and detection strategy is proposed in Fig. 2(c). The process of postmodulation is implemented by adding different time-varying dynamic phase factors to each path:

$$\varepsilon_n(t) = \pi f_{wn} t,$$
$$|f_n(t)\rangle = \frac{1}{\sqrt{2}}(e^{i\varepsilon_n(t)}|0\rangle + e^{-i\varepsilon_n(t)}|1\rangle), \qquad (6)$$

where f_{wn} is the varying frequency of the phase factor on the nth postselection path. Correspondingly, we have

$$p_{fn}(t) = \frac{\langle\phi_{fn}(t)|\hat{p}|\phi_{fn}(t)\rangle}{\langle\phi_{fn}(t)|\phi_{fn}(t)\rangle}. \qquad (7)$$

After a duration time of T, the mean value of $\langle p_{fn}\rangle_T$ is obtained as

$$\langle p_{fn}\rangle_T = \frac{\int_T p_{fn}(t)dN_n}{N_n}, \qquad (8)$$
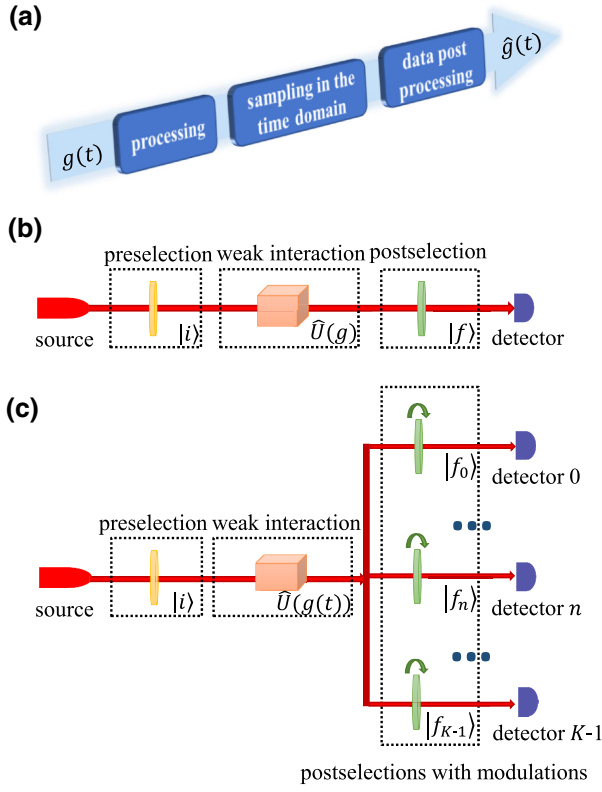
(a)

(b)

(c)

FIG. 2. Schematic diagrams of (a) classical signal processing scheme, (b) standard weak measurement scheme, and (c) our scheme. For our classical signal processing scheme, the signal $g(t)$ is sampled in the time domain after processing, and then the signal is recovered through data postprocessing. In our scheme, the rotating green arrows represent polarization postmodulations of light in multiple paths, where K is the total paths and the nth path has a modulation frequency of f_{wn}.

where N_n and dN_n are the event numbers detected by the nth detector during temporal durations of T and $dt \to 0$, respectively. Moreover, we note that

$$dN_n = N_i P_{sn}(t) dt, \qquad (9)$$

where N_i is the luminous efficiency of light source and $P_{sn}(t) = \langle \phi_{fn}(t) | \phi_{fn}(t) \rangle$ is the probability of a photon being received by the nth detector. Equation (8) can be simplified to

$$\langle p_{fn} \rangle_T = \frac{N_i \int_T \langle \phi_{fn}(t) | \hat{p} | \phi_{fn}(t) \rangle \, dt}{N_n}, \qquad (10)$$

and further expressed as

$$\langle p_{fn} \rangle_T = \frac{N_i p_i}{N_n} \int_T | \langle f_n(t) | i \rangle |^2 dt.$$
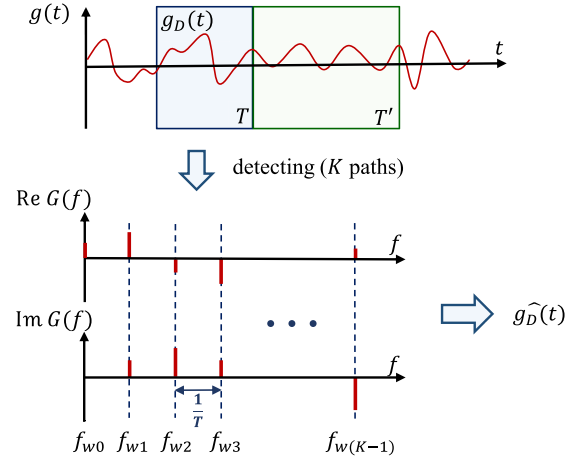

FIG. 3. Schematic diagram of our scheme when estimating a real time-varying parameter. The original signal $g(t)$ is truncated by the time window and becomes the windowed signal $g_D(t)$, and the real and imaginary parts of a frequency point can be obtained at a path in detection. After measurement, $\hat{g}(t)$ can be obtained by connecting $g_D(t)$ in series.

$$+ \frac{2 N_i p^2{}_i}{N_n} \int_T g(t) \mathrm{Im}(\langle i | f_n(t) \rangle \, \langle f_n(t) | \hat{A} | i \rangle) dt$$

$$= \frac{N_i p_i}{2 N_n} \int_T 1 + \cos(2\pi f_{wn} t) dt$$

$$- \frac{N_i p^2{}_i}{N_n} \int_T g(t) \sin(2\pi f_{wn} t) dt, \qquad (11)$$

where $p_i = \langle \phi_i | \hat{p} | \phi_i \rangle$ and $p^2{}_i = \langle \phi_i | \hat{p}^2 | \phi_i \rangle$.

We now demonstrate how to estimate $g(t)$ from Eq. (11). The schematic diagram is depicted in Fig. 3. Since the detection time T is finite, the original signal $g(t)$ is truncated by a rectangular window with a time length of T and an intensity of 1, which can be expressed as

$$g_D(t) = \mathrm{rect}\left(\frac{t - \frac{T}{2}}{T}\right) g(t), \qquad (12)$$

where $\mathrm{rect}[(t - \frac{T}{2})/T]$ is the expression of the rectangular window function.

Estimating on $g_D(t)$ is mathematically equivalent to finding the Fourier series expansion of its period extension $g_T(t)$, which is given by

$$G_T(f_{wn}) = \frac{1}{T} \int_T g(t) \exp(-i 2\pi f_{wn} t) dt. \qquad (13)$$

According to the Euler formula, the real and imaginary parts of $G_T(f_{wn})$ can be given by

$$\text{Im}G_T(f_{wn}) = -\frac{1}{T}\int_T g(t)\sin(2\pi f_{wn}t)dt,$$

$$\text{Re}G_T(f_{wn}) = \frac{1}{T}\int_T g(t)\cos(2\pi f_{wn}t)dt. \tag{14}$$

Thus, the estimated imaginary part of $G_T(f_{wn})$ can be obtained based on Eq. (11):

$$\text{Im}\hat{G_T}(f_{wn}) = \frac{1}{T}\left[\frac{N_n\langle p_{fn}\rangle_T}{N_i{p^2}_i} - \frac{p_i}{2{p^2}_i}\int_T 1 + \cos(2\pi f_{wn}t)dt\right], \tag{15}$$

and the estimated real part of $G_T(f_{wn})$ can be obtained by presetting $\pi/4$ to the phase factor $\varepsilon_n(t)$:

$$\text{Re}\hat{G_T}(f_{wn}) = \frac{1}{T}\left[\frac{p_i}{2{p^2}_i}\int_T 1 - \sin(2\pi f_{wn}t)dt - \frac{N_n\langle p_{fn}\rangle_T}{N_i{p^2}_i}\right]. \tag{16}$$

According to the Fourier analysis theory [2], the spectrum of $g_T(t)$, which needs to satisfy the Dirichlet condition, is composed of base band and harmonic frequency points. The values of f_{wn} are chosen by

$$f_{wn} = n\frac{1}{T}(n \in N), \tag{17}$$

and $g_T(t)$ can be estimated by

$$\hat{g_T}(t) = \sum_{n=-\infty}^{+\infty} G_T\hat{}\left(\frac{n}{T}\right)\exp\left(i2\pi\frac{n}{T}t\right)$$

$$= \sum_{n=-\infty}^{+\infty}\left[\left[\text{Re}\hat{G_T}\left(\frac{n}{T}\right) + i\text{Im}\hat{G_T}\left(\frac{n}{T}\right)\right]\right.$$

$$\times \left.\left[\cos\left(2\pi\frac{n}{T}t\right) + i\sin\left(2\pi\frac{n}{T}t\right)\right]\right]. \tag{18}$$

Correspondingly, $g_D(t)$ can be estimated by intercepting a period of $\hat{g_T}(t)$:

$$\hat{g_D}(t) = \text{rect}\left(\frac{t-\frac{T}{2}}{T}\right)\hat{g_T}(t)$$

$$= \text{rect}\left(\frac{t-\frac{T}{2}}{T}\right)\left\{\sum_{n=-\infty}^{+\infty}\left[\left[\text{Re}\hat{G_T}\left(\frac{n}{T}\right)\right.\right.\right.$$

$$\left.\left.\left. + i\text{Im}\hat{G_T}\left(\frac{n}{T}\right)\right]\left[\cos\left(2\pi\frac{n}{T}t\right) + i\sin\left(2\pi\frac{n}{T}t\right)\right]\right]\right\}. \tag{19}$$

In particular, usually $g(t)$ is real, so $\hat{g_D}(t)$ can be simplified as

$$\hat{g_D}(t) = \text{rect}\left(\frac{t-\frac{T}{2}}{T}\right)\left[\hat{G_T}(0)\right.$$

$$+ 2\sum_{n=1}^{+\infty}\left[\text{Re}\hat{G_T}\left(\frac{n}{T}\right)\cos\left(2\pi\frac{n}{T}t\right)\right.$$

$$\left.\left. - \text{Im}\hat{G_T}\left(\frac{n}{T}\right)\sin\left(2\pi\frac{n}{T}t\right)\right]\right]. \tag{20}$$

Finally, the estimated time-varying parameter $\hat{g}(t)$ can be obtained by connecting $\hat{g_D}(t)$ in series. Furthermore, as the detection time T is flexible, it can be adjusted to afford different frequency resolution [3,18].

In order to precisely evaluate the performance of our scheme, we introduce three figures of merit, i.e., the correlation coefficient, root-mean-square error, and mean absolute error [21–23]. Firstly, the correlation coefficient evaluates the similarity between the true value and estimation value of the parameter, which is defined as follows:

$$r = \frac{\sum_{j=1}^m [g(t_j) - \overline{g(t)}][\hat{g}(t_j) - \overline{\hat{g}(t)}]}{\sqrt{\sum_{j=1}^m [g(t_j) - \overline{g(t)}]^2}\sqrt{\sum_{j=1}^m [\hat{g}(t_j) - \overline{\hat{g}(t)}]^2}}, \tag{21}$$

where $g(t_j)$ and $\hat{g}(t_j)$ are, respectively, the true value and the estimated value of the time-varying parameter at the time of t_j, with $\overline{g(t)}$ and $\overline{\hat{g}(t)}$ being their average values over the whole detection time. On the other hand, the root-mean-square error and the mean absolute error are both used for evaluating the estimation errors, which are defined as follows:

$$E_{\text{rmse}} = \sqrt{\frac{1}{m}\sum_{j=1}^m [g(t_j) - \hat{g}(t_j)]^2}, \tag{22}$$

$$E_{\text{mae}} = \frac{1}{m}\sum_{j=1}^m |g(t_j) - \hat{g}(t_j)|. \tag{23}$$

A good estimation of $g(t)$ requires r being close to 1, and E_{rmse} and E_{mae} being close to 0. As the analytical results are difficult to derive, we perform the analysis with the help of numerical simulations.

III. NUMERICAL SIMULATIONS

A. Analysis without noise

In this section, numerical simulations are applied to demonstrate the advantages of our scheme with comparison of the classical signal processing scheme. For the classical scheme, the signal is sampled in the time domain with

different sampling frequency f_d, and the spline interpolation method (a signal reconstruction function in MATLAB) is applied to reconstruct the signal. On the other hand, the numerical simulation of our scheme is designed based on the reject selection sampling method [24].

For convenience, we focus on the example of time-delay estimation [25–27]. We assign the parameter g as an optical time delay and $\hat{p}$ as the optical angular frequency. As depicted in Fig. 1(c), photons emitted from a light source are modulated to be a linear superposition state of two orthogonal polarizations by the preselection. A time-varying time delay $g(t)$ is introduced by passing through a birefringent element due to the external signal. The evolved photons are postselected after beam splitting, and detected by spectrometers. $g(t)$ can be estimated by calculating the number of photons and the average frequency of the received light, as shown in Eqs. (15) and (16). According to the condition of $|g(t)|p_i \ll 1$, $g(t)$ is set of the order of 10^{-17} s and $\hat{p}$ of the order of 10^{15} Hz. Moreover, g varies with time as

$$g(t) = 1 + \sin\left(2\pi f_s t + \frac{\pi}{3}\right) + 2\sin\left(4\pi f_s t - \frac{\pi}{5}\right)$$
$$+ 3\sin\left(6\pi f_s t - \frac{\pi}{7}\right) + 4\sin(8\pi f_s t). \quad (24)$$

Here, the units of $g(t)$ and t are attoseconds and microseconds, respectively.

The numerical simulation results are shown in Fig. 4. Here we set $f_s = 0.5$ MHz; therefore the maximum frequency component of $g(t)$ is $f_{s(\max)} = 2$ MHz, which means the Nyquist sampling limit on the sampling frequency of the detector (denoted as f_d) is 4 MHz.

For the classical interpolation scheme, the time-varying parameter cannot be correctly revealed when the sampling frequency of the detector is lower than 4 MHz [see Figs. 4(a)–4(c)], which agrees with the Nyquist theorem (the sampling frequency is usually 2.56–4 times the maximum signal frequency in practice [2,3]). For our scheme, the single-shot detecting duration T is set to be 2 μs, corresponding to a sampling frequency of 0.5 MHz. Even with such a low sampling frequency, the time-varying parameter can be perfectly revealed, as is shown in Fig. 4(d).

The results of a comparison between the classical interpolation scheme and our scheme using these three figures of merit are summarized in Table I. It clearly shows that our scheme outperforms the classical interpolation scheme even when the sampling frequency of the detector is set to be much lower than the Nyquist sampling limit.

Indeed, our scheme is the application of the Fourier series expansion, which is the optimal expansion of the error energy [28]. Based on this point of view, there are two cases depending on whether the signal is derivable. On the one hand, if the signal is derivable, the spectrum has finite discrete points. In this case, the advantage of our
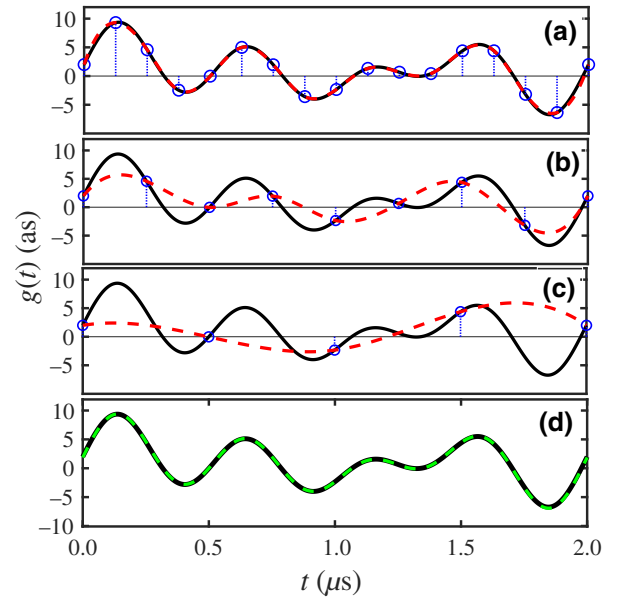

FIG. 4. Numerical simulation results of different detection schemes. The results of the classical interpolation scheme with sampling frequency of 8 MHz (a), 4 MHz (b), and 2 MHz (c). The black lines represent the original time-varying parameter, the blue dotted lines with circles represent the sampling points, and the red dashed lines represent the estimated parameter. (d) The result of our scheme with sampling frequency of 0.5 MHz. The black line is the original time-varying parameter and the green dashed line is the estimated parameter.

scheme is illustrated by the numerical simulation described above, and the time-varying parameter estimation can be well realized as long as the corresponding frequency is detected. One the other hand, if the signal satisfies the Dirichlet condition but there are underivable points, the spectrum has infinite discrete points. In practice, the number of multiple postmodulations and detections is finite, but the performance of our scheme will not be significantly affected when the expansion of time-varying parameters contains a large number of frequencies.

TABLE I. Calculation results of errors and similarity for estimated signals in different schemes.

Scheme	r	E_{rmse} (as)	E_{mae} (as)
Classical interpolation scheme, $f_d = 2$ MHz	0.0589	3.4369	4.6304
Classical interpolation scheme, $f_d = 4$ MHz	0.7806	2.4349	2.1466
Classical interpolation scheme, $f_d = 8$ MHz	0.9984	0.2203	0.1245
Our scheme, $f_d = 0.5$ MHz	0.9999	0.0710	0.0519

To simplify the analysis, we consider the case of real signals, $g_T(t)$, which can be expressed as

$$g_T(t) = G(0) + 2\sum_{n=1}^{+\infty}\left[\text{Re}G_T\left(\frac{n}{T}\right)\cos\left(2\pi\frac{n}{T}t\right)\right.$$
$$\left. - \text{Im}G_T\left(\frac{n}{T}\right)\sin\left(2\pi\frac{n}{T}t\right)\right] \quad (25)$$

in the ideal case and expressed as

$$g_T(t) = G(0) + 2\sum_{n=1}^{K-1}\left[\text{Re}G_T\left(\frac{n}{T}\right)\cos\left(2\pi\frac{n}{T}t\right)\right.$$
$$\left. - \text{Im}G_T\left(\frac{n}{T}\right)\sin\left(2\pi\frac{n}{T}t\right)\right] \quad (26)$$

in the practical case, where K is the number of postmodulations and detections. Correspondingly, the estimation error energy can be expressed as [28]

$$E_K(t) = 2\sum_{n=K}^{+\infty}\left[\text{Re}G_T\left(\frac{n}{T}\right)^2 + \text{Im}G_T\left(\frac{n}{T}\right)^2\right], \quad (27)$$

which indicates that the estimation results are acceptable when the requirement of the estimation error energy is satisfied. In other words, our scheme is effective when K is set to make the signal energy acceptable, and the density of signal frequency points distribution in this frequency band will not affect the scheme. Thus, our scheme is valid if the energy of $g_T(f)$ is mainly concentrated in the bandwidth of $(0, (K-1)/T)$. Indeed, we just have to design K according to the energy requirements of different applications.

Furthermore, in all these cases, our scheme performs always better than sampling the signal in the time domain. When sampling the signal in the time domain in a finite time $\ddot{T}$, its frequency spectrum can be written as [29]

$$G(n\Delta f) = \sum_{m=0}^{M-1} g(mT_d)e^{-j2\pi mn\Delta fT_d}, \quad (28)$$

where mT_d is the mth sampling point, $n\Delta f$ is the nth frequency point, and the total number of m and n is M. The sampling frequency $f_d = 1/T_d = M\Delta f = M/\ddot{T}$ acts with the effect of spectrum truncation [29], which means a fixed M in the error energy:

$$E_M(t) = 2\sum_{n=M}^{+\infty}\left[\text{Re}G_T\left(\frac{n}{\ddot{T}}\right)^2 + \text{Im}G_T\left(\frac{n}{\ddot{T}}\right)^2\right]. \quad (29)$$

For our scheme, the spectrum truncation is controlled by setting the number of paths K. Comparing Eq. (27) with Eq. (29), it always has a smaller estimation error energy by setting $K > M$ if the integration time T is set as the same
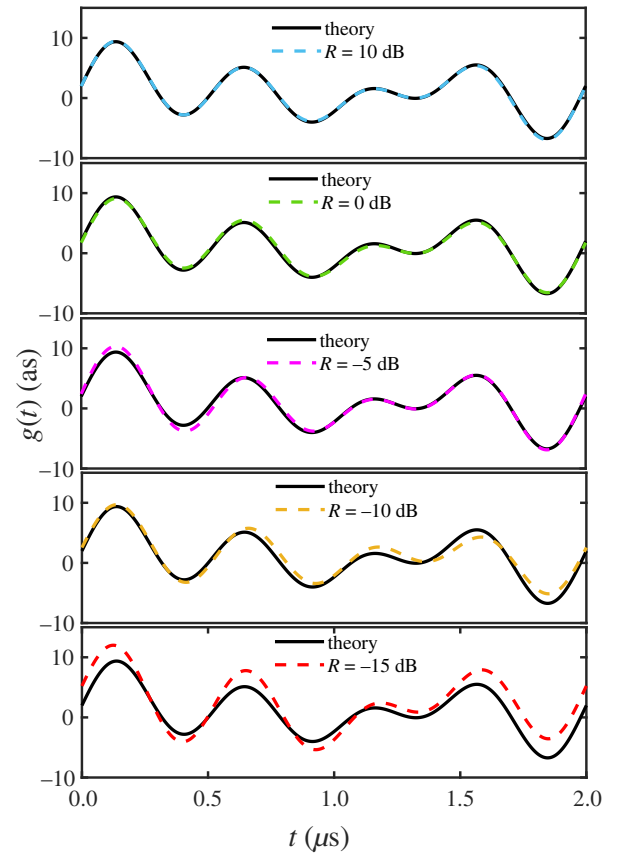

FIG. 5. Estimation results of the time-varying parameter accompanied by white noise at different levels. The black solid line is the original signal and the dashed lines in different colors represent the estimation results for different values of R: the red, yellow, purple, green, and blue dashed lines are the estimated signals for $R = -15$ dB, $R = -10$ dB, $R = -5$ dB, $R = 0$ dB, and $R = 10$ dB, respectively.

as the finite time $\ddot{T}$. Moreover, the integration time T in our scheme is arbitrary, which can be lengthened or shortened. In other words, a smaller K can have the same effect by setting a shorter T_j, where $\ddot{T} = T_1 + T_2 + \cdots + T_j + \cdots$ and connected T_j in order after estimation.

B. Analysis with white noise

To demonstrate the validity of our scheme under a noisy environment, we further calculate the figure of merit when a random variation is added in Eq. (24), i.e.,

$$g(t) = 1 + \sin\left(2\pi f_s t + \frac{\pi}{3}\right) + 2\sin\left(4\pi f_s t - \frac{\pi}{5}\right)$$
$$+ 3\sin\left(6\pi f_s t - \frac{\pi}{7}\right) + 4\sin(8\pi f_s t) + \Delta g(t)$$
$$= g_p(t) + \Delta g(t). \quad (30)$$

For simplicity, we assume $\Delta g(t)$ to be a Gaussian white noise. We quantify the size of the time-varying parameter

TABLE II. Calculation results of errors and similarity for the estimated parameters in white noise environment of different levels.

Situation	r	E_{rmse} (as)	E_{mae} (as)
Noise-free	0.9999	0.0710	0.0519
$R = 10$ dB	0.9997	0.1032	0.0787
$R = 0$ dB	0.9976	0.2777	0.2398
$R = -5$ dB	0.9949	0.4664	0.3219
$R = -10$ dB	0.9798	0.8694	0.7443
$R = -15$ dB	0.9443	2.0382	1.7401

in comparison with the random variation with ratio R:

$$R = 10 \log \left(\frac{\int_T |g_p(t)|^2 dt}{\int_T |\Delta g(t)|^2 dt} \right), \qquad (31)$$

the unit of which is dB.

The estimation results are depicted in Fig. 5, and the corresponding values of r, E_{rmse}, and E_{mae} are shown in Table II. The simulation results show that our scheme maintains good performance even when R reduces to -5 dB, which implies its robustness to white noise.

IV. CONCLUSION

In summary, we propose a high-precision time-varying parameter estimation scheme based on weak measurement with postmodulations. Unlike previous schemes, our scheme performs signal sampling in the frequency domain by postmodulation of the predetected signal instead of a postprocessing of data. By doing so, our scheme is able to surpass the Nyquist sampling limit and effectively avoid aliasing distortion. Numerical simulations show that our scheme outperforms the classical interpolation scheme with sampling frequency much lower than the Nyquist sampling limit, and maintains high performance in a white noise environment with R as low as -5 dB. As the estimation of a time-varying parameter is a special task of function estimation, our work may provide a method for quantum metrology of functions [30].

ACKNOWLEDGMENTS

[1] H. Nyquist, Certain topics in telegraph transmission theory, Trans. Am. Inst. Electr. Eng. **47,** 617 (1928).

[2] J. Zheng, Q. Ying, and W. Yang, *Signal and System* Vol. 1 (Higher Education Press, Beijing, 2011), 3rd ed.

[3] A. V. Oppenheim and R. W. Schafer, *Discrect-Time Signal Processing* (Xian Jiao Tong University Press, Shaanxi, 2015), 3rd ed.

[4] T. Wu, R. Hu, X. Wang, and S. Ke, Audio object coding based on optimal parameter frequency resolution, Multimed. Tools Appl. **78,** 20723 (2019).

[5] C. Hu, X. Wang, R. Hu, and Y. Wu, Audio object coding based on N-step residual compensating, Multimed. Tools Appl. **80,** 18717 (2021).

[6] Z. Ren, J. Hu, and H. Tang, *et al.*, Optimization method of electro-optical imaging system based on information distortion, J. Appl. Opt. **38,** 689 (2017).

[7] C. G. Davis, K. S. Lorenz, J. Goodman, G. Stantchev, L. Boglione, and B. D. Nousain, Alias-free products of signals near Nyquist rate, IEEE Trans. Signal Process. **66,** 4151 (2018).

[8] G. He, J. Han, L. Liang, and J. Xiao, in *Journal of Physics: Conference Series*, Vol. 1605 (IOP Publishing, 2020), p. 012106..

[9] M. Mishali and Y. C. Eldar, Blind multiband signal reconstruction: Compressed sensing for analog signals, IEEE Trans. Signal Process. **57,** 993 (2009).

[10] X. Chen, E. A. Sobhy, Z. Yu, S. Hoyos, J. Silva-Martinez, S. Palermo, and B. M. Sadler, A sub-nyquist rate compressive sensing data acquisition front-end, IEEE J. Emerging Sel. Top. Circuits Syst. **2,** 542 (2012).

[11] D. Cohen, D. Cohen, Y. C. Eldar, and A. M. Haimovich, Summer: Sub-Nyquist MIMO radar, IEEE Trans. Signal Process. **66,** 4315 (2018).

[12] R. Arie, A. Brand, and S. Engelberg, Compressive sensing and sub-Nyquist sampling, IEEE Instrum. Meas. Mag. **23,** 94 (2020).

[13] N. Fu, Z. Wei, L. Qiao, and Z. Yan, Short-observation measurement of multiple sinusoids with multichannel sub-Nyquist sampling, IEEE Trans. Instrum. Meas. **69,** 6853 (2020).

[14] X. Luo and Z. Zhang, Data recovery with sub-Nyquist sampling: Fundamental limit and a detection algorithm, Front. Inf. Technol. Electron. Eng. **22,** 232 (2021).

[15] C. Herley and P. W. Wong, Minimum rate sampling and reconstruction of signals with arbitrary frequency support, IEEE Trans. Inf. Theory **45,** 1555 (1999).

[16] R. Venkataramani and Y. Bresler, Perfect reconstruction formulas and bounds on aliasing error in sub-Nyquist nonuniform sampling of multiband signals, IEEE Trans. Inf. Theory **46,** 2173 (2000).

[17] M. Mishali and Y. C. Eldar, From theory to practice: Sub-Nyquist sampling of sparse wideband analog signals, IEEE J. Sel. Top. Signal Process. **4,** 375 (2010).

[18] X. Zhang, *Modern Signal Analysis and Processing* (Tsinghua University Press, Beijing, 2018).

[19] Y. Aharonov, D. Z. Albert, and L. Vaidman, How the Result of a Measurement of a Component of the Spin of a Spin-1/2 Particle Can Turn Out To Be 100, Phys. Rev. Lett. **60,** 1351 (1988).

[20] J. Dressel, M. Malik, F. M. Miatto, A. N. Jordan, and R. W. Boyd, Colloquium: Understanding quantum weak values: Basics and applications, Rev. Mod. Phys. **86,** 307 (2014).

[21] X. Shao, X. Kang, X. Wang, X. Yuan, and G. Lu, Comprehensive evaluation index of wavelet denoising quality

based on multiinformation fusion, J. Ordnance Equipment Eng. **41**, 155 (2002).

[22] K. Tao and J. Zhu, A hybrid indicator for determining the best decomposition scale of wavelet denoising, Acta Geodaetica et Cartographica Sinica **41**, 749 (2012).

[23] Y. Chen, L. Chen, H. Liu, K. Wang, and X. Yang, Determination of the optimal decomposition scale in wavelet de-noising of optical fiber sensing signal, J. Optoelectron. Laser **24**, 2372 (2013).

[24] L. Xu, *Mathematic Dictionary* Vol. 4 (Shanxi Education Press, Shanxi, 2002).

[25] N. Brunner and C. Simon, Measuring Small Longitudinal Phase Shifts: Weak Measurements or Standard Interferometry?, Phys. Rev. Lett. **105**, 010405 (2010).

[26] J. Huang, Y. Li, C. Fang, H. Li, and G. Zeng, Toward ultrahigh sensitivity in weak-value amplification, Phys. Rev. A **100**, 012109 (2019).

[27] C. Fang, J. Huang, Y. Yu, Q. Li, and G. Zeng, Ultra-small time-delay estimation via a weak measurement technique with post-selection, J. Phys. B: At., Mol. Opt. Phys. **49**, 175501 (2016).

[28] A. V. Oppenheim, A. S. Willsky, and S. H. Nawab, *Signals & Systems* (Xian Jiao Tong University Press, Shaanxi, 1998), 2nd ed.

[29] J. Zheng, Q. Ying, and W. Yang, *Signal and System* Vol. 2 (Higher Education Press, Beijing, 2011), 3rd ed.

[30] N. Kura and M. Ueda, Standard Quantum Limit and Heisenberg Limit in Function Estimation, Phys. Rev. Lett. **124**, 010507 (2020).